



POLITECNICO DI TORINO  
Repository ISTITUZIONALE

WALL SHEAR STRESS TOPOLOGICAL SKELETON IDENTIFICATION IN CARDIOVASCULAR FLOWS: A PRACTICAL APPROACH

*Original*

WALL SHEAR STRESS TOPOLOGICAL SKELETON IDENTIFICATION IN CARDIOVASCULAR FLOWS: A PRACTICAL APPROACH / Mazzi, Valentina; Gallo, Diego; Calo', Karol; Khan, Muhammad O.; Steinman, David A.; Morbiducci, Umberto. - ELETTRONICO. - (2019). ((Intervento presentato al convegno Summer Biomechanics, Bioengineering, and Biotransport Conference tenutosi a Seven Springs (PA) nel 25/06/2019-28/06/2019.

*Availability:*

This version is available at: 11583/2743653 since: 2019-07-26T15:11:12Z

*Publisher:*

Summer Biomechanics, Bioengineering, and Biotransport Conference

*Published*

DOI:

*Terms of use:*

openAccess

This article is made available under terms and conditions as specified in the corresponding bibliographic description in the repository

*Publisher copyright*

(Article begins on next page)

## WALL SHEAR STRESS TOPOLOGICAL SKELETON IDENTIFICATION IN CARDIOVASCULAR FLOWS: A PRACTICAL APPROACH

Valentina Mazzi (1), Diego Gallo (1), Karol Calò (1), Muhammad O. Khan (2),  
David A. Steinman (3), Umberto Morbiducci (1)

(1) Polito<sup>BIO</sup>Med Lab, Department of  
Mechanical and Aerospace Engineering  
Politecnico di Torino  
Turin, Italy

(2) Cardiovascular Biomechanics  
Computation Lab, Department of Pediatrics  
Stanford University  
Stanford, CA, USA

(3) Biomedical Simulation Laboratory, Department of  
Mechanical & Industrial Engineering  
University of Toronto  
Toronto, ON, Canada

### INTRODUCTION

The observed co-localization of “disturbed” hemodynamics and atherosclerotic lesion prevalence has led to the identification of low and oscillatory Wall Shear Stress (WSS) as a biomechanical localizing factor for vascular dysfunction [1]. However, recent evidences have underlined how consideration of only “low and oscillatory” WSS may oversimplify the complex hemodynamic milieu to which the endothelium is exposed.

In this context, recent studies have highlighted the relevance of WSS fixed points, and the stable and unstable manifolds that connect them [2][3]. These WSS topological features have a strong link with flow features like flow stagnation, separation, and recirculation, which are usually classified as “disturbed” flow. Technically, a fixed point of a vector field is a point where the vector field vanishes, while unstable/stable vector field manifolds identify contraction/expansion regions linking the fixed points. The set of fixed points and their connections form the topological skeleton of a vector field. The presence of WSS fixed points and of WSS contraction/expansion regions, highlighted by WSS manifolds, might induce focal vascular responses relevant for, e.g., early atherosclerosis, or, aneurysm rupture [3]. For these reasons, the topological skeleton analysis of the WSS vector field is of great interest and motivates the study present herein.

Lagrangian techniques have been recently proposed to identify WSS manifolds but have certain practical limitations [2]. An Eulerian approach has also been suggested, but only for 2D analytical fields [4]. Here we propose and demonstrate the use of a simple Eulerian approach for identifying WSS topological skeleton on 3D surfaces.

### METHODS

Ten carotid bifurcation computational hemodynamics models from the Vascular Aging-The Link That Bridges Age to Atherosclerosis

(VALIDATE) study were considered. Details on geometry reconstruction, personalized conditions at boundaries and CFD simulations are reported elsewhere [5].

Based on Volume Contraction theory, it can be demonstrated that the computation of the divergence of a vector field gives practical information about the associated dynamical system, avoiding numerical integration for manifolds identification, as required for Lagrangian technique, thus significantly reducing the computational effort. In particular, the divergence is able to (1) encase the connections between attractors and (2) identify the basins of attractions of each attractor. For this reason, here we used a divergence-based approach for WSS manifolds identification at the luminal surface of carotid bifurcations.

As WSS divergence depends by construction upon the algebraic summation of the *magnitude* of the single gradients of WSS vector components, in some cases it might fail in properly identify WSS expansion/contraction regions. In fact, these regions describe specific directional arrangements of the vectors, but both variations in magnitude and in directions are taken into account in the divergence. Consequently, here the divergence of the normalized WSS vector field was proposed:

$$\text{DIV}(\boldsymbol{\tau}_{\mathbf{u}}) = \nabla \cdot \left( \frac{\boldsymbol{\tau}}{\|\boldsymbol{\tau}\|_2} \right), \quad (1)$$

where  $\boldsymbol{\tau}_{\mathbf{u}}$  is the WSS unit vector. Eq. (1), neglecting the vector field magnitude variation but taking into account variation of directions of the vector field, correctly identifies WSS manifolds and is suitable for practical WSS topological analysis at the luminal surface of an arterial segment.

To complete the analysis, we propose a robust method to WSS fixed points identification at the luminal surface. The Poincarè index is considered here for WSS fixed points identification because of its mesh-independent and topologically invariant proprieties. Once identified, a

Jacobian analysis of WSS fixed points allows then to classify the fixed point attractive or repelling nature. The proposed practical approach for the WSS topological skeleton identification is applied to both cycle-average and instantaneous WSS vector fields.

The cycle-average WSS vector field at the luminal surface  $\bar{\boldsymbol{\tau}}(\mathbf{x})$  is

$$\bar{\boldsymbol{\tau}}(\mathbf{x}) = \frac{1}{T} \int_0^T \boldsymbol{\tau}(t, \mathbf{x}) dt \quad (2)$$

where T is the cardiac cycle duration. It was previously suggested that cycle-average WSS vector field  $\bar{\boldsymbol{\tau}}$  fixed points and their associated manifolds influence the near-wall intravascular transport [2]. However, the paradoxical observation that a  $\bar{\boldsymbol{\tau}}$  fixed point would have never been a real instantaneous fixed point (i.e., a null vector) along the cardiac cycle, calls into question the real physical meaning of fixed points of the cycle-average WSS vector field. In fact, from the definition of the Time-Average Wall Shear Stress (TAWSS) and from the Integral Inequality Absolute Value it follows that:

$$|\bar{\boldsymbol{\tau}}(\mathbf{x})| = \left| \frac{1}{T} \int_0^T \boldsymbol{\tau}(t, \mathbf{x}) dt \right| \leq \frac{1}{T} \int_0^T |\boldsymbol{\tau}(t, \mathbf{x})| dt = \text{TAWSS}(\mathbf{x}) \quad (3)$$

suggesting that a null value for  $|\bar{\boldsymbol{\tau}}|$  does not necessarily imply the same for TAWSS. Moreover, it can be easily demonstrated that a null value for TAWSS at a specific location implies the existence there of a fixed point along all cardiac cycle. Eq. (3) highlights the need for a practical method for an in-depth analysis of the kinematics of instantaneous WSS fixed points along the cardiac cycle. Hence, WSS fixed points analysis is applied here to instantaneous WSS vector field and a measure to quantify the fraction of cardiac cycle spent by instantaneous WSS fixed points at a specific location at the luminal surface is proposed:

$$RT_{x_{fp}}(e) = \frac{\bar{A}}{A_e} \frac{1}{T} \int_0^T \mathbb{I}_e(\mathbf{x}_{fp}, t) dt \quad (4)$$

where  $\mathbf{x}_{fp}(t)$  is the WSS fixed point position at time  $t \in [0, T]$ ,  $e$  is the generic triangular element of the superficial mesh of area  $A_e$ ,  $\bar{A}$  the average surface area of all triangular elements of the superficial mesh and  $\mathbb{I}$  is the indicator function.

## RESULTS

An analytical vector field was used for benchmarking purposes. The proposed method was compared to the classical vector field integration approach [6] and to the recent trajectory-free method [4], providing excellent results. Then, the cycle-average WSS vector field at the luminal surface of the 10 carotid bifurcation models was analyzed. The topological skeleton of the cycle-average WSS vector field of one explanatory carotid bifurcation model, including fixed points and stable/unstable manifolds is presented in Figure 1.

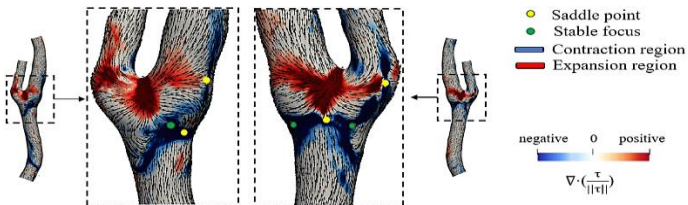


**Figure 1: Topological skeleton of cycle-average WSS vector field.**

The contraction and expansion patterns, identifying unstable and stable manifolds, represent the basins of attraction for the stable fixed points associated with the manifolds. Notably, all cycle-average WSS fixed points identified using the Poincaré index at the luminal surface of the 10 carotid bifurcation models were located within contraction regions, thus confirming the appropriateness of the proposed method. For an in-depth characterization of the WSS fixed points, the quantity  $RT_{x_{fp}}(e)$ , as defined in Eq. (4), was computed on the surface of all the carotid bifurcation models and an explanatory example is presented in Figure 2. For visualization purposes, regions of interest  $R_{fp}$  were identified at the luminal surface around high  $RT_{x_{fp}}(e)$  areas and including the

identified cycle-average WSS fixed points locations (labeled from  $A_C$  to  $G_C$ ). For the explanatory model presented in Figure 2, the results of the WSS fixed points residence times analysis are summarized in Table 1 and clearly show that: (1) in regions  $R_{E_C}$  and  $R_{G_C}$  fixed points residence times were up to 30% of the cardiac cycle; (2) instantaneous WSS fixed points resided for small fractions of the cardiac cycle (range 0.0-14.5%) in cycle-average WSS fixed points identified locations; (3) interestingly, in the cycle-average WSS stable focus  $B_C$  location, the instantaneous WSS vector presented both saddle point (2%) and stable focus (2.9%) configurations along the cardiac cycle; (4) in regions  $R_{D_C}, R_{E_C}, R_{F_C}$  instantaneous WSS fixed points were always of the same type as cycle-average WSS fixed points; (5) paradoxically, it emerged that at position  $C_C$  where a cycle-average WSS saddle point was identified, the instantaneous WSS vector never presented a fixed point along the cardiac cycle (we remind here that a WSS fixed point represents a focal point at the luminal surface subject to an atheroprone hemodynamic environment).

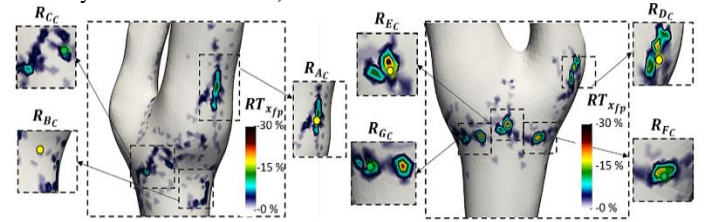


**Figure 2: Map of fixed points residence time  $RT_{x_{fp}}(e)$ .**

$R_{fp}$	Instantaneous WSS fixed points nature in $R_{fp}$	Cycle-Average WSS fixed point nature in $R_{fp}$	Instantaneous WSS fixed points residence time at cycle-average WSS fixed point location in $R_{fp}$
$R_{A_C}$	SPs and SFs	SP ( $A_C$ )	3.4% SPs, 0% SFs
$R_{B_C}$	SPs and SFs	SF ( $B_C$ )	2% SPs, 2.9% SFs
$R_{C_C}$	SPs and SFs	SP ( $C_C$ )	0% SPs, 0% SFs
$R_{D_C}$	SPs	SP ( $D_C$ )	1.5% SPs, 0% SFs
$R_{E_C}$	SPs	SP ( $E_C$ )	14.5% SPs, 0% SFs
$R_{F_C}$	SFs	SF ( $F_C$ )	0% SPs, 12.5% SFs
$R_{G_C}$	SPs and SFs	SF ( $G_C$ )	0% SPs, 8.2% SFs

**Table 1: Summary of WSS fixed points kinematics. SPs and SFs denote Saddle Points and Stable Foci, respectively.**

## DISCUSSION

A practical approach to fixed points and manifolds identification was presented and applied to cardiovascular flows. The proposed approach requires the vector field and its divergence only and it can be easily implemented for 3D vector field defined on complex geometries. This practical way to analyze instantaneous WSS fixed points along the cardiac cycle allows to evaluate their residence time and how strong is local contraction/expansion using WSS divergence (data not shown). Our findings on carotid bifurcation models question the physical significance of WSS fixed points on cycle-average WSS fields, and suggest instead a focus on their dynamics. In conclusion, the practical approach proposed here could contribute to speed up studies on the physiological significance of fixed points in cardiovascular flows, in the context of the increasing interest as expressed by recent literature on this still-poorly-explored argument.

## REFERENCES

- [1] Morbiducci, U. et al., *Thromb Haemost*, 15: 484- 492,20016.
- [2] Arzani, A. et al., *Biomech. M. Mechanobiol.*, 16:787-803, 2016.
- [3] Arzani, A. et al., *J Biomech*, 73: 145-152, 2018.
- [4] Gary, K. et al, *Nonlinear Dynamics*, 2018.
- [5] Gallo, D. et al, *Ann Biomed Eng*, 43(1): 68-81, 2015.
- [6] Gambaruto, A.M et al, *Computer& Fluids*, 65:56-65, 2012.